

The Stiffness of Collagen Fibrils Influences Vascular Smooth Muscle Cell Phenotype

Dennis P. McDaniel,* Gordon A. Shaw,[†] John T. Elliott,* Kiran Bhadriraju,[‡] Curt Meuse,* Koo-Hyun Chung,[†] and Anne L. Plant*

*Biochemical Science Division and [†]Manufacturing Metrology Division/National Institute of Standards and Technology, Gaithersburg, Maryland 20899; and [‡]SAIC, Arlington, Virginia 22203

ABSTRACT Cells receive signals from the extracellular matrix through receptor-dependent interactions, but they are also influenced by the mechanical properties of the matrix. Although bulk properties of substrates have been shown to affect cell behavior, we show here that nanoscale properties of collagen fibrils also play a significant role in determining cell phenotype. Type I collagen fibrils assembled into thin films provide excellent viewing of cells interacting with individual fibrils. Cells can be observed to extensively manipulate the fibrils, and this behavior seems to result in an incompletely spread stellate morphology and a nonproliferative phenotype that is typical of these cells in collagen gels. We show here that thin films of collagen fibrils can be dehydrated, and when seeded on these dehydrated fibrils, smooth muscle cells spread and proliferate extensively. The dehydrated collagen fibrils appear to be similar to the fully hydrated collagen fibrils in topology and in presentation of β_1 integrin ligation sites, but they are mechanically stiffer. This decrease in compliance of dehydrated fibrils is seen by a failure of cell movement of dehydrated fibrils compared to their ability to rearrange fully hydrated fibrils and from direct measurements by nanoindentation and quantitative atomic force measurements. We suggest that increase in the nanoscale rigidity of collagen fibrils can cause these cells to assume a proliferative phenotype.

INTRODUCTION

Cells interact with their extracellular matrix (ECM) proteins primarily through integrin receptors (1,2), which lead to activation of downstream signaling and cytoskeleton organization. Although specific integrin receptors interact with specific ECM proteins through chemical recognition, mechanical properties of the ECM environment also play a large role in intracellular signaling and cell response. How cells respond to the changing mechanical properties in their environment is likely critical to development, differentiation, and the etiology of disease (2–9).

A number of studies have examined cellular response to bulk mechanical properties of polymeric materials. Studies have examined the effect of substrate compliance on cell spreading and motility using polymeric matrices with variable cross-linking to variable rigidity (10,11). Such studies allowed estimation of traction forces and indicated that on less rigid matrices cells are less spread, are more motile, and have more dynamic focal adhesions than cells on stiffer matrices. Measurements of the forces that cells can exert can be made using micropatterned polymeric materials where deflection of the polymer allowed precise calculation of force applied (12,13). Such studies showed that the forces exerted by cells, on the order of tens of nanonewtons, are greater for more highly spread cells. Cells also appear responsive to

very small (piconewton) resistance on subcellular length scales (12,14).

Several studies have also shown that cell responses may depend on how the matrix is presented to cells. For example, on fibrillar collagen surfaces, cell migration and the recruitment of myosin II-B to membrane protrusions appeared to be dramatically different from on nonfibrillar collagen (15). The importance of the supramolecular structure of collagen fibrils in determining cell phenotype has been directly demonstrated in our laboratory (16–18) as well as by others (19–21). These studies show that vascular smooth muscle cells (vSMCs) and fibroblasts respond with different phenotypes to fibrillar collagen I compared to nonfibrillar collagen I even when in both cases cell-matrix ligation occurs through the β_1 integrin. These results have led us to speculate that collagen fibrils provide topographical and/or mechanical features that are important determinants of cell phenotype.

VSMCs cultured on thick collagen gels are often used as a model system to study the role of the extracellular matrix in vascular diseases. The ligation of vSMCs to type I fibrillar collagen occurs through the β_1 integrin receptor ($\alpha_1\beta_1$ and $\alpha_2\beta_1$) and results in incomplete spreading, a stellate appearance, and a low rate of proliferation (22–24). We have previously described thin films of collagen and have shown that morphology, proliferation rates, integrin ligation, and tenascin-C expression of vSMCs are nearly identical whether cells are on thin films of collagen or on thick gels of collagen (16,17). The thin films consist of a submicron-thick bed of collagen fibrils and result from the self-assembly of monomeric collagen from solution into supramolecular fibrils at an alkanethiol-covered surface. Thin films of collagen have

Submitted May 17, 2006, and accepted for publication November 14, 2006.

Address reprint requests to Anne L. Plant, Biochemical Science Division, Chemical Science and Technology Laboratory, National Institute of Standards and Technology, Gaithersburg, MD 20899. Tel.: 301-975-3124; Fax: 301-975-8246; E-mail: anne.plant@nist.gov.

© 2007 by the Biophysical Society

0006-3495/07/03/1759/11 \$2.00

doi: 10.1529/biophysj.106.089003

many advantages over thick gels, including reproducibility, ease of characterization, robustness, and spatial homogeneity. Furthermore, the thinness of the films gives the matrix excellent optical properties, and so interactions between the filopodia of the cells and the fibrils are easily seen by optical microscopy.

Another important advantage of thin films of collagen is that their properties can be systematically manipulated in ways that are difficult to do with thick gels. Previously, to determine the importance of the supramolecular structure of the collagen fibrils to the normal vSMC phenotype, we prepared thin films from solutions of relatively high concentrations of collagen (from which large fibrils form) and from solutions of low concentrations of collagen (from which collagen adsorbs but does not form supramolecular fibrillar structures) (16). In this study, we show that the mechanical properties of collagen fibrils change as a result of dehydration. After dehydration, individual fibrils are significantly stiffer and less compliant, as evidenced by quantitative small force measurements using nanoindentation and atomic force microscopy (AFM). In response to the increase in stiffness of the fibrils, cells spread more and become more proliferative compared to cells on flexible, fully hydrated fibrils. With this experimental system, mechanical properties of fibrils and the effect on cells can be examined without altering integrin recognition or topography. These data show that the nanoscale mechanical properties of collagen fibrils influence cellular phenotype.

METHODS

Indication of specific manufacturers and products is for clarity only and does not constitute endorsement by the National Institute of Standards and Technology (NIST).

Preparation and treatment of collagen films

Collagen thin films were prepared as described previously (16). Briefly, acid-washed coverslips were coated with a 5-nm layer of chromium and a 15–20-nm layer of gold by magnetron sputtering. Coated coverslips were then placed in a 0.5-mM solution of 1-hexadecanethiol in ethanol for at least 8 h before being rinsed with ethanol and dried with filtered N₂ gas. These alkanethiol-coated coverslips were then incubated in neutralized solutions (0.3 mg/ml) of native type I bovine collagen (Vitrogen, Cohesion Technologies, Palo Alto, CA) at 37°C overnight. After incubation, the samples were lifted out of the collagen solution and rinsed with Dulbecco's phosphate buffered saline (DPBS) and deionized water from Teflon squirt bottles. After rinsing, the collagen-coated coverslips were dried very briefly under a stream of filtered N₂ gas. This brief drying of the thin film can be observed with reflected light and typically takes ≈30 s. Light microscopy shows that if this brief drying is omitted, the collagen fibrils of which the thin film is composed appear to be anchored at one end to the surface, with the other end apparently floating free in solution. Cells seeded onto this film of vertical collagen fibrils fail to spread to typical size and undergo apoptosis (data not shown). The brief 30-s drying results in a horizontal meshwork of collagen fibrils.

In this study, thin films referred to as fully hydrated were immediately immersed in DPBS after this brief drying period, and samples referred to as dehydrated were placed in the back of the laminar flow hood and allowed to remain dry for 24–48 h or other times as indicated. All thin films were

incubated with culture media for a minimum of 15 min before seeding with cells to allow protein adsorption from the serum-containing media.

Cell culture

The rat aortic vSMC line A10 (vSMC; ATCC, Manassas, VA) was maintained in Dulbecco's Modified Eagles Medium (DMEM; Mediatech, Herndon, VA) supplemented with nonessential amino acids, glutamine, penicillin (100 units/ml), streptomycin (100 µg/ml), HEPES buffer (25 mM), and 10% (v/v) fetal bovine serum (FBS; Gibco Invitrogen, Carlsbad, CA), and maintained in a humidified 5% (v/v) CO₂ balanced-air atmosphere at 37°C. Subconfluent cultures were switched to DMEM containing 2% (v/v) FBS 24 h before an experiment. Cells were removed from the polystyrene tissue culture flasks by trypsinization, washed with DMEM containing 2% (v/v) FBS, and plated in DMEM containing 2% (v/v) FBS onto the collagen thin film substrates at a density of 2,000 cells/cm², a density at which cell-to-cell contact is minimized.

Serum-free defined media were prepared by adding to DMEM 1 µL/mL each of insulin and human epidermal growth factor (Clonetics, San Diego, CA; mammary epithelium growth medium singlequots), and 5 nM lysophosphatidic acid (Sigma, St. Louis, MO).

Light microscopy and image analysis

All light microscopy was performed on an Olympus IX70 inverted microscope (Olympus America, Melville, NY) equipped with motorized shutters, filter wheels, and stage for x, y, and z axis position control (Ludl Electronic Products, Hawthorne, NY) and controlled by ISee imaging software (ISee Imaging Systems, Cary, NC). For live cell studies, cells were maintained at 37°C in either a Biotechs FCS2 closed chamber system (Biotechs, Butler, PA) or an incubator system that encloses the entire microscope stage (Solent Scientific, Portsmouth, UK). Images of live cells were recorded every 30 s, processed in ImageJ (National Institutes of Health, Bethesda, MD), and converted into movies using QuickTime (Apple, Cupertino, CA) for presentation.

Cells were fixed and stained and examined by automated microscopy as previously described (25). Briefly, cells were washed in 37°C Hank's buffer containing 25 mM HEPES and then immersed in 4% (v/v) formaldehyde in DPBS for 1 h. After fixation, cells were rinsed with DPBS and fluorescently labeled with Texas Red maleimide to label the whole cell and DAPI to label the nuclei. This fluorescent labeling allows automated determinations of cell area using a custom routine written for ImageJ.

Proliferation assay

Cellular proliferation was quantified as described previously (17). Briefly, both fully hydrated and dehydrated collagen thin films were prepared in individual wells of eight-well plates. To these thin films, vSMCs were seeded at a density of 1,100 cells/cm² and incubated at 37°C. After 24 h, all wells were washed twice with fresh media to remove unadhered cells, and fresh media were added before returning plates to the incubator. After an additional 1 h incubation, the first thin films were fixed. The remaining thin films were fixed 48, 72, and 96 h after seeding. All thin films containing cells were stained immediately after fixation. Automated fluorescence microscopy was used to image 50 fields of view of each thin film preparation, and automated analysis of the resulting images was used to determine cell densities. Two replicate thin films were examined for each preparation and time point examined. An increase in the number of cells per unit area over time provided a quantitative determination of cell proliferation.

Antibody blocking

For antibody blocking studies, cells were trypsinized to release them from the polystyrene culture flask and resuspended in DMEM containing

2% (v/v) FBS. To these suspended cells was added either 10 $\mu\text{g/ml}$ anti- β_1 integrin antibody (Fitzgerald Industries International, Concord, MA), 10 $\mu\text{g/ml}$ of a control IgM (BD Biosciences, San Jose, CA), or no antibody. Cells were gently agitated periodically to keep them in suspension for 15 min during antibody incubation and then were plated in triplicate at a density of 2,000 cells/cm² on both fully hydrated and dehydrated collagen thin films. After 2 h, cells were fixed and fluorescently labeled for morphological analysis.

Topographical AFM

For topographical AFM (PicoScan; Molecular Imaging, Phoenix, AZ) thin films of collagen were prepared on chromium- and gold-coated silicon wafers. Images are shown for collagen thin films imaged in air or in aqueous phosphate buffered saline (PBS). Samples were imaged using Si tips in a magnetically driven, intermittent contact mode. Images were flattened with the PicoScan software to improve visualization.

Quantitative AFM

A Molecular Force Probe three-dimensional (3D) AFM (Asylum Research, Santa Barbara, CA) was used to image and perform mechanical testing in the small force regime, using a BioLever (Olympus, Tokyo) microfabricated gold-coated silicon nitride cantilever probe (with a nominal tip radius of ≈ 40 nm). All tests were conducted in the NIST Advanced Measurement Laboratory in a low-grade clean room environment where ambient temperature was set at 20°C and controlled within 0.02°C. All quantitative AFM measurements were performed under PBS. A small force was applied normal to the fibril surface with the AFM cantilever tip while the resulting displacement from the force applied to the fibril surface was measured. Contact stiffness of fibrils, k_f , was determined using the relationship (26)

$$k_f = k_c / (s/s_f - 1),$$

where k_c , the spring constant of the cantilever, was determined using the thermal method to be 0.031 N/m with an uncertainty of $\sim 10\%$ (27,28). The parameter, s , is the optical lever arm sensitivity measured from AFM curves of photodetector voltage, ΔV , versus the distance, Δz , moved by the piezo on a hard surface, and is defined as

$$s = \Delta z / \Delta V.$$

The parameter, s_f , is the corresponding optical lever arm sensitivity measured for the collagen sample. Values for s_f were estimated directly from plots of cantilever deflection versus position of the z axis sensor. Although the curves indicated a more complex function, a linear model was assumed for simplification. The slope was measured from the plots by drawing a line from a point on the curve at the z axis position that corresponded to a force of 100 pN to a point on the curve corresponding to a displacement of 200 nm in z .

For consistency, measurements were made on single fibrils in areas where they appeared not to be in contact with other fibrils and appeared to be lying close to the solid support. Force-displacement curves were systematically collected at five points along the cross section of the fibril (see Supplemental Material Fig. 4). At the edges of a fibril, the force curves typically showed low levels of hysteresis, but near the center of the hydrated fibrils there was significantly more hysteresis. The center of dehydrated fibrils was assumed to be the positions showing greatest deflection of the probe. Multiple measurements made on each fibril were highly reproducible, and 10 different fibrils were measured for each sample. For the estimate of s_f , we selected the force curves that corresponded to a tip position near the center of the fibril.

Nanoindentation

Instrumented indentation tests were performed using a Triboscope indenter (Hysitron, Minneapolis, MN) housed in a stainless steel enclosure with an

encoded translation sample stage. To map topographical features of the sample surface, the Berkovich indenter tip (radius 100–200 nm) was raster scanned across the sample surface using a Nanoscope IIIa AFM controller (Digital Instruments, Santa Barbara, CA). In a previous study, the indenter apparatus was calibrated with SI-traceable deadweight loading so that absolute force accuracy is within 1% from 50 μN to 5000 μN (29). All tests were conducted in the NIST Advanced Measurement Laboratory in a low-grade clean room environment where temperature was controlled to within 0.02°C. All force measurements were performed under water; therefore no capillary effects are expected to contribute to the forces measured. When covered in water, the collagen fibrils were not conducive to topographical imaging with this large probe, and so each had to be located manually using the encoded translation stage. To do this, the indenter tip was lowered until just before contact with the sample surface was made. The force output from the indentation transducer was then monitored on an oscilloscope while the sample was translated using the encoded stage. As the indenter contacted a fibril, it would deflect upward enough to be detected on the oscilloscope and then back downward after the indenter passed over the fibril. In this way, the approximate center of the fibril could be located. Once an individual fibril was located, a linearly ramped load was applied to the indenter tip, and its displacement was monitored as it penetrated the fibril surface. The loading rate used for all experiments was 100 $\mu\text{N/s}$, and ~ 30 loading curves were taken for each of the fully hydrated and dehydrated samples.

RESULTS

Thin films of collagen

Thin films of collagen were formed by allowing a neutralized solution of purified Type I bovine collagen monomer to polymerize at an alkanethiol self-assembled monolayer. We have examined various aspects of the formation and structure of these extracellular matrix thin films as well as the response of cells to these matrices as compared to thick collagen gels (16–18). Light microscopy and AFM images are shown in Fig. 1. The predominant features are fibrils ≈ 200 –250 nm in diameter and up to tens of micrometers long. These fibrils are seen in Fig. 1, A–C, by AFM and in Fig. 1 D by differential interference contrast (DIC) light microscopy. Fig. 1 A is of dehydrated fibrils imaged in buffer, and Fig. 1 B is of fully hydrated fibrils imaged in buffer. Images of fully hydrated fibrils show poorer resolution, which is an indication that they are more flexible than dehydrated fibrils and move significantly under the AFM tip. A closer AFM view of a sample obtained by scanning a smaller area in air allows higher resolution imaging of smaller underlying fibrils. These are seen in Fig. 1 C as fibrils ≈ 75 nm in diameter and ≈ 250 -nm long. Other AFM data reported previously (16) suggest that the larger fibrils polymerize from the smaller fibrils as depicted in Fig. 1 E. As can be seen in Fig. 1 D, the collagen fibrils that make up these thin films appear to be homogeneously distributed across the surface. This suggests that all cells seeded onto the surface will experience a similar extracellular environment; i.e., there are no areas with a radically different density or size distribution of fibers.

To further assess the similarities between the fully hydrated and the dehydrated collagen films, we performed a variogram analysis (30) on phase contrast images of hydrated and dehydrated samples derived from Supplemental

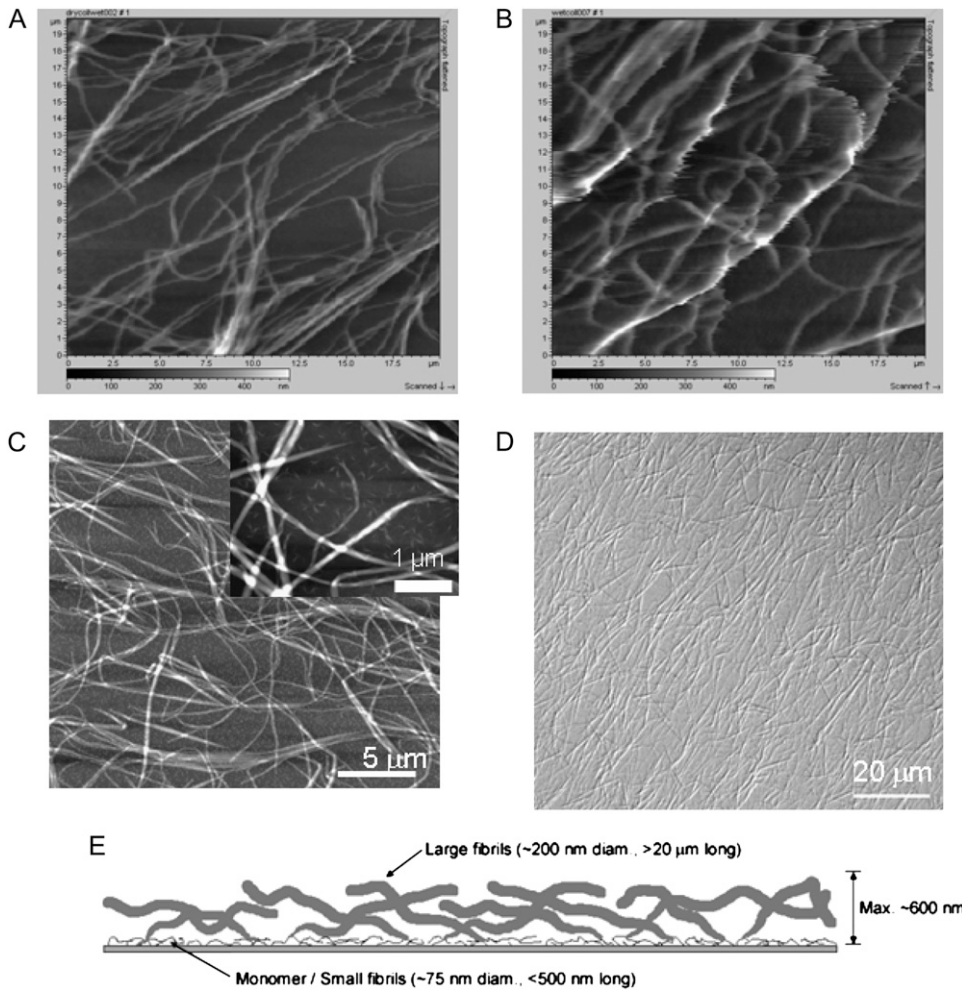


FIGURE 1 Thin films of collagen. (A–C) Topographical AFM shows that the predominant features of collagen thin films are large fibrils ≈ 200 – 250 nm in diameter that correspond to the fibrils visible under the light microscope. (A) Dehydrated collagen film imaged in buffer. Scanned area = $20 \mu\text{m} \times 20 \mu\text{m}$. (B) Fully hydrated collagen film imaged in buffer. Scanned area = $20 \mu\text{m} \times 20 \mu\text{m}$. (C) Collagen film imaged in air; scale bar = $5 \mu\text{m}$. (Inset) A higher resolution scan allows observation of smaller fibrils that underlie the larger fibrils; scale bar = $1 \mu\text{m}$. (D) DIC image of a thin film of fibrillar collagen demonstrating homogeneity of surface coverage; scale bar = $20 \mu\text{m}$. (E) Schematic of the structure of a thin film depicting the hypothesis that small collagen assemblies ranging from monomers to 75 -nm diameter fibrils lie very close to the alkanethiol layer, and larger fibrils grow out of them.

Movie 1. We selected three cell-free regions from each image and calculated the variance between pixel intensities as a function of the distance the pixels are apart along every row of pixels in the region. Large variance differences that occur with high frequency at constant distances will contribute to a large peak at that characteristic distance. In the case of the images of fibrillar collagen, the largest peak is determined by the characteristic distance between the center of the largest fibrils and the center of the areas between fibrils. The largest trough will be the characteristic distance between areas of minimal variance, i.e., the distance between the center of fibrils or the distance between the centers of areas devoid of large fibrils. Representative variogram plots are shown in Supplemental Material Fig. 1. This analysis indicated that the characteristic distance between areas of largest variance (i.e., between the center of fibrils and the center of nonfibrillar areas) was $3.7 \pm 0.4 \mu\text{m}$ for the fully hydrated collagen fibrils and $4.0 \pm 0.2 \mu\text{m}$ for the dehydrated fibrils and that the characteristic distance between areas of least variance or from fibril to fibril or area to area between large fibrils is approximately twice that, $8.5 \pm 1.9 \mu\text{m}$ and $8.3 \pm 1.8 \mu\text{m}$, respectively. This analysis suggests

that the fully hydrated and the dehydrated collagen films are not significantly different topographically.

Cell morphology

Fig. 2 shows cells growing on thin films of fully hydrated (Fig. 2 A) and dehydrated (Fig. 2 B) collagen thin films. Collagen fibrils can be seen under the cells in both images. Despite the fact that the matrix in both samples appears similar, vSMCs display different phenotypes on fully hydrated collagen compared to dehydrated collagen. As can be seen in Fig. 2, A and C, vSMCs cultured on fully hydrated collagen display numerous filopodia and appear to be smaller than those on dehydrated collagen (Fig. 2, B and D), which characteristically display well-formed lamellipodia. To quantify the differences in cellular morphology seen on the different thin films, vSMCs were grown for 24 h on collagen thin films that had been dried for different periods of time, then fixed and fluorescently labeled with Texas Red maleimide. One hundred fields were selected by preprogrammed movements of the stage, and a total of ≈ 1000 cells were imaged on each of three replicates of each collagen

preparation. The area of each cell was determined as described previously (25).

As can be seen in Fig. 2 *E*, a range of cell spread areas was observed for all treatments. Mean cell areas were calculated from the population of cells for each of three replicate experiments. Mean cell area increases with the number of hours that the thin film has been allowed to dehydrate. On fully hydrated thin films (0 h of drying), cells spread to an average area of $2104 \mu\text{m}^2 \pm 116 \mu\text{m}^2$, whereas cells on thin films allowed to dry for 48 h spread to an average area of $4587 \mu\text{m}^2 \pm 104 \mu\text{m}^2$. The average area of cells on thin films of collagen that had been allowed to dry for 1 h was $2280 \mu\text{m}^2 \pm 70 \mu\text{m}^2$, which is not significantly different from cells on the fully hydrated collagen, suggesting that this amount of drying time was not sufficient to alter collagen properties significantly. Fig. 2 *E* also demonstrates that an intermediate average cell area, $3725 \mu\text{m}^2 \pm 295 \mu\text{m}^2$, can be elicited by drying the thin films for an intermediate time of 4 h. The average area of cells on the collagen films allowed to dry for 24 h was $4588 \mu\text{m}^2 \pm 175 \mu\text{m}^2$, which is not significantly different from the average area of cells on collagen films allowed to dry for 48 h, leading to the conclusion that the effects of drying of the thin film are complete after 24 h. In Fig. 2 *F*, the same data that were used to calculate the means in Fig. 2 *E* are shown as histograms, which allows the examination of distribution of cell responses. As we have observed previously (16–18), cells within a population express a highly reproducible range of phenotypes, even though they are genetically identical and are exposed to a spatially homogeneous matrix. In an effort to ensure that the intermediate average cell area measured on the thin film allowed to dry for 4 h did not result from a mixture of small and large cells that might be produced by some parts of the coverslip being dried more thoroughly than others, cell areas were measured on five different locations of the coverslip (each corner and the center) and the distribution of cell areas at each location was nominally the same as that shown in Fig. 2 *F* (data not shown).

Integrin dependence

Interestingly, the average cell area elicited by dehydrated thin films of collagen is very similar to the average area of vSMCs on denatured collagen (16). VSMCs are known to interact with native Type I collagen through the β_1 integrin receptor and with denatured collagen through the $\alpha_v\beta_3$ integrin (31,32). To examine whether drying of the collagen results in a change in integrin recognition, we performed an integrin blocking experiment. Cells were preincubated in suspension for 15 min with either an antibody to the β_1 integrin subunit, an unrelated IgM antibody, or no antibody, and then plated on thin films of fully hydrated and dehydrated collagen fibrils for 2 h. The results of this experiment are seen in Fig. 3. Cells incubated with either no antibody or with an unrelated IgM adhered to both fully hydrated and dehydrated

thin films and spread to an average area of $\sim 2000 \mu\text{m}^2$, whereas cells incubated with the anti- β_1 antibody adhered but failed to spread on both fully hydrated as well as dehydrated thin films. The similarity of response of vSMCs on both the fully hydrated and dehydrated thin films in the presence of the anti- β_1 antibody suggests that integrin recognition of the thin film has not been affected by drying. It should be noted, however, that a large number of cells incubated with the anti- β_1 antibody detach during fixation and washing and that more cells appear to detach from the dehydrated collagen than the fully hydrated collagen. This observation may suggest that there are subtle interactions between the cells and collagen that may not be explained by integrin ligation alone. Nevertheless, it is clear that vSMC adherence and spreading on dehydrated collagen remains dependent on β_1 integrin ligation.

We also examined the spreading of cells on fully hydrated and dehydrated collagen thin films in serum-free medium to ascertain if variable adsorption of serum proteins could account for the different cell response on the two matrices. Cells were applied to the collagen films in serum-free media and their areas quantified after 4 and 24 h. Cells had an average area of $1670 \pm 81 \mu\text{m}^2$ and $2796 \pm 225 \mu\text{m}^2$ after 4 h and $1802 \pm 21 \mu\text{m}^2$ and $3864 \pm 414 \mu\text{m}^2$ after 24 h on fully hydrated and dehydrated collagen, respectively, for $n = 2$ replicate measurements (see Supplemental Material Fig. 2). Thus, even in the absence of serum, the dehydration of collagen resulted in a more spread phenotype, suggesting that differential adsorption of serum components on dehydrated collagen is not sufficient to account for the observed phenotype.

Proliferation

It has been frequently observed that vSMCs on fibrillar collagen assume an incompletely spread stellate appearance, a relatively high degree of motility, and a suppressed rate of proliferation (22–24). Previous experiments in our laboratory have shown that these phenotypic characteristics are displayed by vSMCs on thin films of fibrillar collagen as well as on thick gels of collagen (17). In this study, we compared the ability of vSMCs to proliferate on thin films of dehydrated fibrillar collagen to that for cells on thin films of fully hydrated collagen. The results indicate that dehydration has a dramatic effect on increasing the rate of proliferation. As seen in Fig. 4, vSMCs on fully hydrated thin films did not increase in number over a 96-h period, whereas cells on dehydrated thin films experienced an increase in cell density of $>300\%$ over the same time period.

Cellular manipulation of collagen fibrils

Examination of living vSMCs on fully hydrated collagen over time provides evidence that cells can initiate movements of collagen fibrils on the order of 1–5 μm (Fig. 5, A

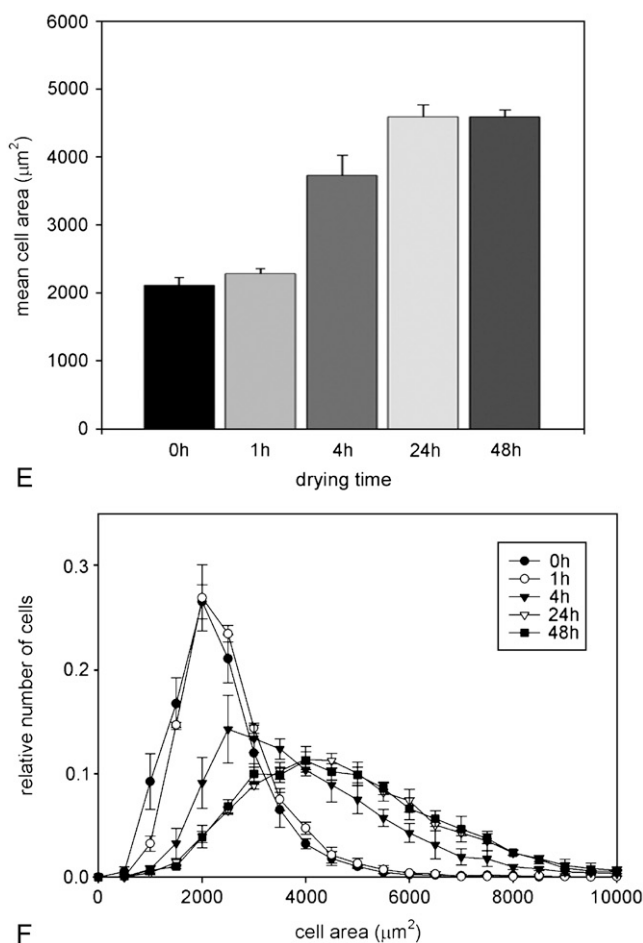
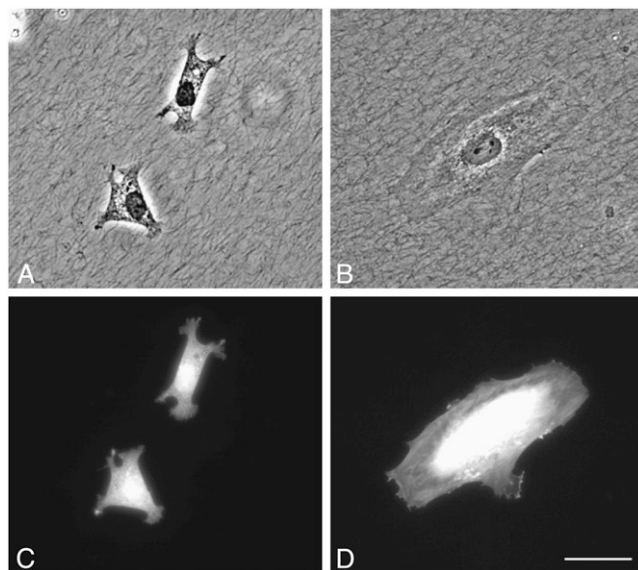


FIGURE 2 Effect of collagen dehydration on vSMC morphology. (A) vSMCs on fully hydrated collagen films are incompletely spread and interact with collagen fibers through filopodia. (B) vSMC on dehydrated collagen films are well spread and form lamellipodia; (C and D). Fluorescence micrographs of the same cells seen in A and B, respectively, stained with Texas Red maleimide. Scale = 50 μm . (E) Mean cell area of vSMCs after 24 h on collagen thin films prepared with no dehydration (0 h) or different

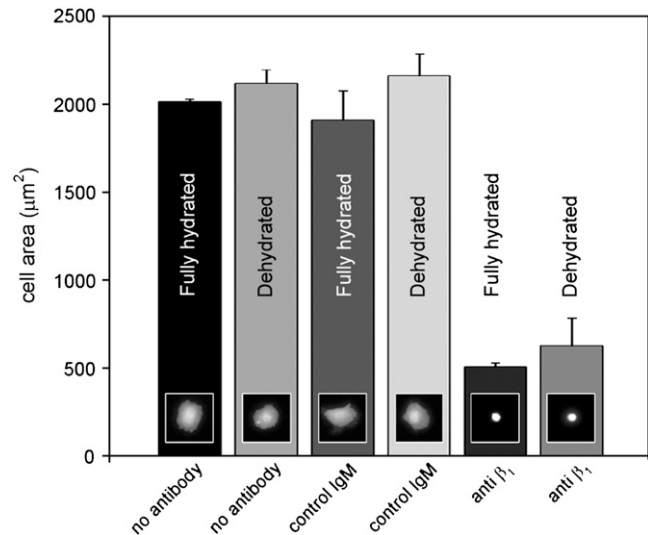


FIGURE 3 Effect of anti- β_1 integrin function-blocking antibody. vSMCs were preincubated for 15 min with either no antibody, a nonspecific control IgM, or a function-blocking anti- β_1 antibody. Cells were then plated on either fully hydrated collagen or dehydrated collagen and allowed to spread for 2 h. Cells on dehydrated collagen require ~ 6 h to reach their fully spread area and so were not fully spread at the end of this experiment. Error bars represent the standard deviation of three replicate experiments. Small inset fluorescence micrographs depict a typical cell from each experimental condition.

and B, and Supplemental Movies 1 and 2). In addition, the net movement of fibrils is apparent from optical sectioning in the z axis. Fig. 5 C shows a cell that was grown on a fully hydrated collagen thin film for 48 h. Some areas in the immediate vicinity of the cell show extensive rearrangement of large fibrils. A series of images collected on an axis perpendicular to the image plane shows that some of these missing fibrils appear to have been translocated to the top of the cell body as shown in Fig. 5, C–E. Movement of dehydrated collagen fibrils by cells was never observed. The difference in cell interaction with fully hydrated and dehydrated collagen fibrils can be seen by comparison of Supplemental Movies 2 and 3.

Nanoindentation studies

Antibody-blocking studies indicate that the cells interact with both fully hydrated and dehydrated collagen through the β_1 integrin receptor, suggesting that chemical differences in the collagen matrix are unlikely to be the cause of the different phenotypes. Furthermore, the observations of cell-initiated movement of fully hydrated collagen fibrils and the apparent lack of movement of dehydrated fibrils suggest

periods of dehydration before seeding cells. Error bars represent the standard deviation of three replicate experiments. (F) Histograms of distributions of cell areas after different drying times. The legend indicates the numbers of hours the thin film was allowed to remain dry before seeding cells. Error bars represent the standard deviation of three replicate experiments.

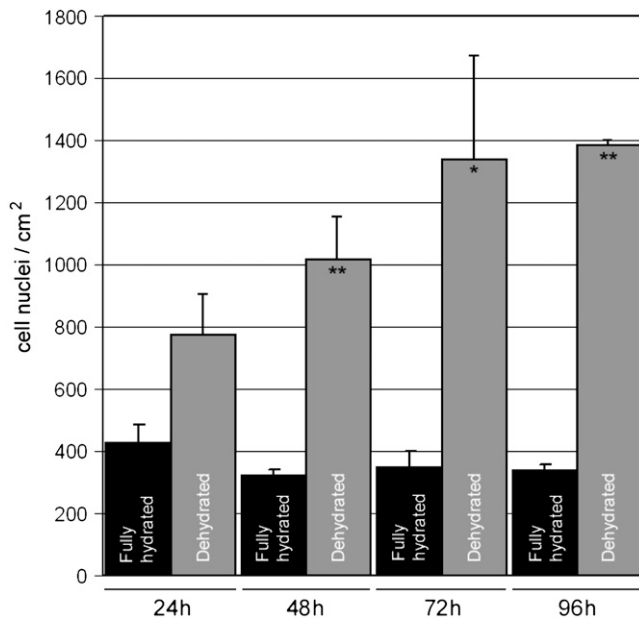


FIGURE 4 Effect of dehydration of collagen on cell proliferation. The number of cells on fully hydrated collagen did not increase over a 96-h period, whereas cell population on dehydrated collagen increased more than 300% over 96 h. ** = $p < 0.01$ between fully hydrated and dehydrated collagen. * = $p < 0.05$ between fully hydrated and dehydrated collagen. Error bars represent SD of two replicates.

that the mechanical properties of the collagen fibrils are changed during dehydration. To directly test the effects of dehydration on the mechanical properties of collagen fibrils, we employed nanoindentation and quantitative AFM.

In nanoindentation, the tip approaches the surface at a constant rate, and as it presses into the sample, the load and

displacement of the tip are recorded and used to calculate properties such as hardness and elasticity. Because in this study the radius of the nanoindenter tip is on the order of the thickness of the fibril being probed (≈ 100 – 200 nm), this measurement is sensitive to the larger scale forces responsible for the integrity of fibrils and the forces between the fibril and its substrate. Fig. 6 shows representative force-displacement curves generated at fully hydrated and dehydrated fibrils. A distinct plateau region is seen in both plots, as marked by the arrows, indicating the occurrence of rupture of individual collagen fibrils. To verify that these plateaus correspond to the rupturing of the collagen fibrils, an indentation test was performed in air. In this condition, the fibrils can be imaged easily, and an individual fibril located, indented, and imaged again to inspect the condition of the fibril after indentation. It was observed that very little damage occurred to the fibril if a load less than that necessary to cause the observed force plateau was applied. However, if a load greater than that necessary to cause the plateau was applied, the fibril appeared to be cut, as can be seen in the topographical images of Fig. 6.

Forces required for rupture are significantly different for the fully hydrated and the dehydrated fibrils. A larger force, $322 \pm 18 \mu\text{N}$, is required to rupture the fully hydrated fibrils compared to $266 \pm 17 \mu\text{N}$ to rupture the dehydrated fibrils. It is apparent that the plateau region in the data for fully hydrated collagen fibrils is not as sharp as that for the dehydrated fibrils. This suggests that the rupture of hydrated fibrils is not as abrupt, perhaps because they are more flexible than and not as brittle as dehydrated fibrils. Lower forces of up to $100 \mu\text{N}$ could be applied repeatedly to both fully hydrated and dehydrated fibrils without causing rupture of the fibrils (Fig. 6 A, inset). The $100\text{-}\mu\text{N}$ indents vanished

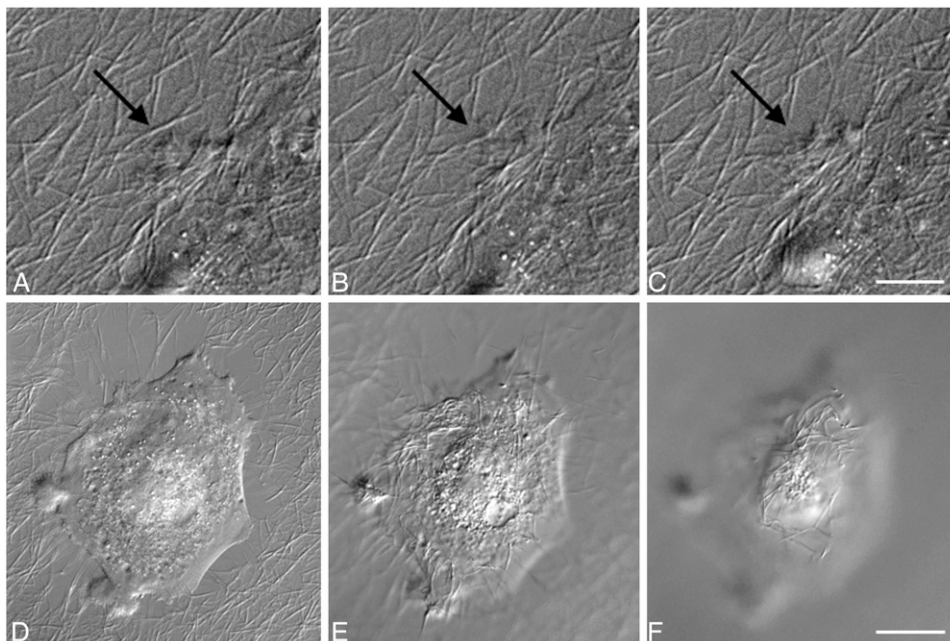


FIGURE 5 DIC micrographs of vSMCs on fully hydrated collagen thin films showing manipulation of fibrils by cells. (A–C) Sequential images of the periphery of the cell showing fibril movement due to cell action. A moved fibril is indicated by the arrow, which is in the same location in all images. Interval between frames = 6 min. Scale = $10 \mu\text{m}$. (D–F) A series of images taken perpendicular to the plane of focus showing a cell on a fully hydrated collagen thin film after 48 h growth. (D) Areas immediately around the cell appear to be denuded of large fibrils. (E and F) Fibrils have accumulated on the dorsal surface of the cell. Scale = $20 \mu\text{m}$.

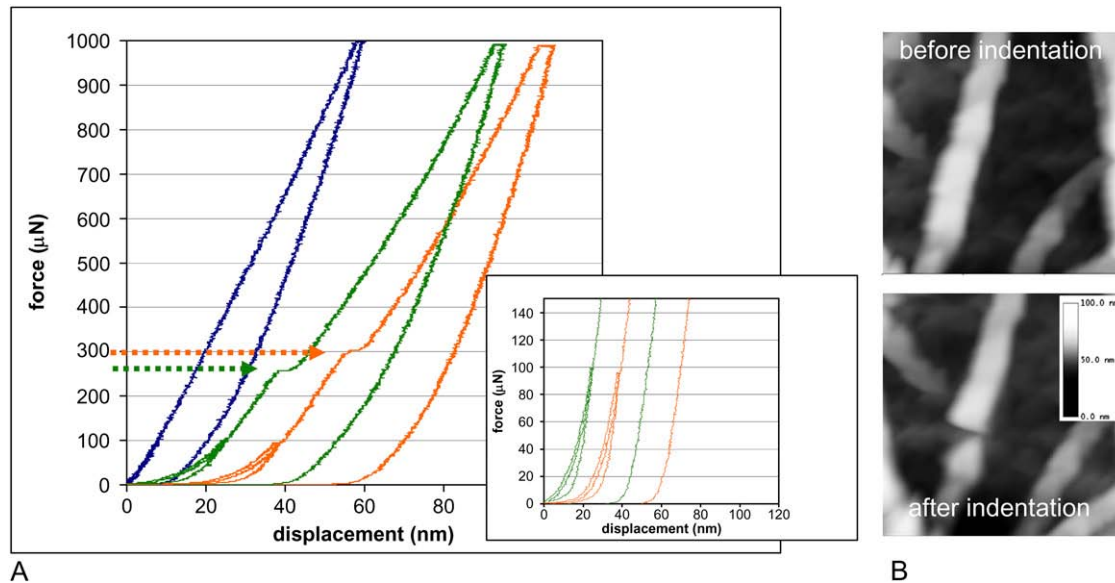


FIGURE 6 Nanoindentation of fully hydrated and dehydrated collagen fibrils. (A) Representative force-displacement curves before and during nanoindentation of dehydrated (green) and fully hydrated (orange) collagen fibrils. Abrupt excursions in the loading profile during fibril rupture are indicated by arrows. A force of $322 \pm 18 \mu\text{N}$ is required to rupture the fully hydrated fibrils compared to $266 \pm 17 \mu\text{N}$ to rupture the dehydrated fibrils; 30 different fibrils were measured for each sample. Forces up to $100 \mu\text{N}$ could be applied repeatedly without damage to the fibrils (inset). The blue curve represents a typical scan from an area between large fibrils (which is populated by the very small fibrils from which large fibrils arise); similar data were observed whether the sample was fully hydrated or dehydrated. (B) A dehydrated collagen fibril in a thin film before (top) and after (bottom) application of force with the nanoindenter. This image was taken in air, but indentation results were comparable to the force-displacement curves of the dehydrated samples measured under water. Although the fibril is poorly resolved because of the large tip radius, it is still clear that rupture of the fibril occurred.

almost completely upon unloading, indicating that under these forces fibrils deform but recover.

Quantitative AFM

The quantitative AFM data also show distinct differences between the fully hydrated and dehydrated collagen in the low force loading regime. The smaller scale of the AFM tip (radius $\approx 40 \text{ nm}$) allows analysis of smaller scale mechanical features that are closer to the molecular scale. Representative force-displacement curves generated with the AFM tip are shown in Fig. 7 together with an AFM image of the areas being probed. For these measurements, we examined areas where a fibril appeared not to be in close contact with another fibril and appeared to be close to the solid support. As seen in Fig. 7, the force-displacement curves for dehydrated fibrils were very different from those for the fully hydrated fibrils. The dehydrated fibrils show a relatively smooth and steep transition of force with displacement and little hysteresis. In contrast, the fully hydrated fibrils show a relatively shallow slope as the tip contacts the fibril, and the slope increases with distance moved by the cantilever. This increase in slope could be the result of forces associated with inter- and/or intra-fibrillar interactions. Significant hysteresis is associated with the unloading curves for the fully hydrated fibrils, which could reflect adhesion of fibrils to the underlying surface or perhaps a slow relaxation of deformation of the fibril.

Repeated force displacement curves in the same place on fibrils indicated a high degree of reproducibility, suggesting that the low forces applied did not permanently damage the fibrils. The z axis displacement of fully hydrated fibrils by the applied force is significantly greater than displacement of dehydrated fibrils. At the highest forces, both fully hydrated and dehydrated fibrils show little deflection in response to increasing force, suggesting that the fibrils are at that point unable to further compress and the underlying solid support is contributing strongly to the force curve.

We approximated fibril stiffness by assuming a linear relationship between applied force and displacement at low force loads. Using this assumption, we estimated the effective contact stiffness of the fibrils in PBS to be $3 \times 10^{-3} \text{ N/m} \pm 2 \times 10^{-3} \text{ N/m}$ and $3 \times 10^{-2} \text{ N/m} \pm 2 \times 10^{-2} \text{ N/m}$ for the fully hydrated and dehydrated fibrils, respectively. These values are the results of measurements of 10 different fibrils and therefore indicate the variability observed between different fibrils. These data indicate that there is on average an order of magnitude difference in the mechanical stiffness of the fully hydrated and dehydrated collagen fibrils.

DISCUSSION

In this study we used thin films of collagen fibrils to examine the effect of nanoscale mechanical properties on phenotypic responses of vSMCs. Previous studies with vSMCs (16,17)

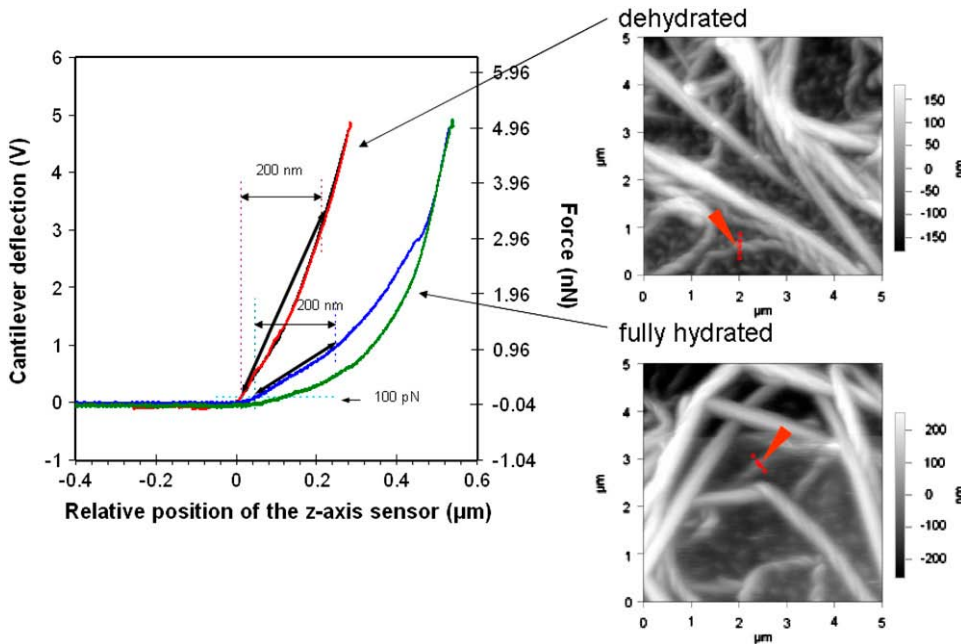


FIGURE 7 Force versus displacement with quantitative AFM. An AFM tip with a radius of ≈ 40 nm was used to probe collagen fibrils that were kept fully hydrated (loading curve in blue and retraction in green) and the corresponding AFM image, or were dried extensively (loading curve in red and retraction in black) and the corresponding image. Measurements were taken in PBS. Five force-displacement curves of each fibril were taken at different points that span the width of the fibrils as indicated by the arrows in the images. See Supplementary Material Fig. 4, *a* and *b*, for examples of these systematic measurements. The curves shown here correspond to a position near the center of each fibril. The parameter s_f was estimated from a linearization of the loading curves as described in Methods and was used to calculate the contact stiffness, k_f .

and with fibroblasts (18) have shown that thin films of fibrillar collagen provide a matrix to cells that is highly analogous to that of collagen gels. On fully hydrated collagen fibrils, vSMCs exhibit a poorly spread, nonproliferative phenotype, just as they do on thicker collagen gels (16,17). Thin films provide opportunities for manipulating the matrix in systematic ways. For example, we have previously studied how collagen solution concentration influences the supramolecular structure of surface collagen and the resulting response of cells (16). In the absence of large (≈ 200 nm) supramolecular assemblies of collagen fibrils, cells spread extensively and become proliferative. These previous results, together with results of others (19–21) suggest that the supramolecular structure of nondenatured collagen and mechanical forces associated with fibrils influence cellular phenotype. The study reported here was designed to examine directly the effect of mechanical properties of collagen fibrils on vSMC growth and spreading.

Thin films of collagen also provide excellent optical properties for light microscopy, allowing better visualization of cell interaction with collagen fibrils. Lateral movements of fully hydrated collagen fibrils of 1–5 μm can be observed, and the translocation of fully hydrated fibrils by cells to their dorsal surfaces suggests that the thin films provide an environment similar to a 3D matrix. The effect of increasing the stiffness of the collagen fibrils results in failure of cells to manipulate the matrix as seen in Supplemental Movies 1–3. These observations indicate that dehydration of fibrils alters the ability of vSMCs to manipulate them and suggest that dehydration affects the mechanical properties of the fibrils.

How the mechanical properties of collagen are influenced by dehydration has been addressed in many studies. Rheological studies suggest that loss of water from collagen fibrils

results in tighter packing of fibrils and enhanced mechanical rigidity due to increased interfibril attractive forces (34). These observations appear to be consistent with theory and experiment on the elasticity and rigidification of hydrogels with swelling and dehydration (35,36). Raman spectroscopy indicates a role for hydration layers in maintaining the spacing within collagen fibrils (37). Other studies have examined the effect of chemical cross-linking and found an inverse relationship between hydration of collagen and degree of cross-linking (38,39). Molecular dynamics simulations with a collagen-like peptide indicate that the absence of water produces an increase in the number of intramolecular hydrogen-bonds (40). High-resolution crystal structure data indicate that hydrogen-bonding occurs in collagen through a large number of hydration sites (41) that form both interchain and intrachain bridges. These H-bonds appear to be intrinsic features of collagen triple helices, and their dynamics indicate that they are kinetically labile and can exchange readily (42).

To begin to understand the molecular changes that accompany dehydration of collagen fibrils, we have examined collagen thin films by infrared reflection spectroscopy and observed significant differences in the spectra of fully hydrated and dehydrated collagen films in the amide I region. We observed a major peak at 1655 cm^{-1} in fully hydrated collagen films that was replaced by a transition at 1643 cm^{-1} in the dehydrated collagen films (see Supplemental Fig. 3). Amide I shifts from 1660 to 1630 cm^{-1} have been attributed to strengthening and shortening of hydrogen-bonds within the triple helix during the process of fibril formation (43). At completion of fibril formation, the higher frequency transition dominated again, indicating that a more relaxed, less rigid structure of the collagen triple helix could be tolerated in the intact fibril (43). Based on these results, our observation

that the amide I peak shifts to lower frequencies in dehydrated collagen is consistent with a more rigid molecular structure with shorter hydrogen-bonds. We also observed differences when fully hydrated and dehydrated samples were exposed to deuterated water; amide-deuterium (N-D) stretches increased in fully hydrated collagen fibrils over time for ~ 20 min, but little N-D exchange occurred in dehydrated fibrils. N-D intensities were an order of magnitude smaller in dehydrated samples. Together, these data suggest that dehydrated fibrils may experience closer H-bonding and have restricted access to solvent, which would be consistent with restricted molecular mobility.

Using nanoindentation and quantitative AFM, we also directly observed mechanical differences in brittleness and in contact stiffness between fully hydrated and dehydrated collagen fibrils. We suggest that the increased stiffness of the dehydrated fibrils allows cells to exert more mechanical tension on the matrix, which potentiates the proliferative phenotype. Apparent mean contact stiffness of individual fully hydrated fibrils in PBS was estimated to be $3 \text{ nN}/\mu\text{m}$, which is an order of magnitude less than the $30 \text{ nN}/\mu\text{m}$ estimated for dehydrated fibrils. The quantitative AFM technique measures resistance to force applied normal to an individual fibril. Nevertheless, the magnitude of these contact stiffness values is similar to compliance values reported by others. Using a polyacrylamide gel and measuring compliance by deformation from a hanging weight, a value of $46 \text{ nN}/\mu\text{m}$ was found to cause fibroblasts to be less spread and more motile compared to cells exposed to matrix with a compliance of $730 \text{ nN}/\mu\text{m}$ (10). In another study (7), a difference of polymer compliance of a factor of 2 was sufficient to result in differences in phenotype. Unlike studies that have examined the effect of bulk polymer materials, the data in this study suggest that nanoscale mechanical properties of individual ECM fibrils are responsible for determining phenotypic parameters such as cell spreading and proliferation in vSMCs. Similarly, the role of mechanical response to single collagen fibrils was demonstrated by Meshel et al. (15).

The intracellular signaling pathways that are responsible for the differences in vSMC response to hydrated and dehydrated collagen films are currently under investigation in our laboratory. A difference in adsorption of serum components on the two different films appears not to be a determinant of the phenotypic differences since we observed similar behavior under serum-free, defined media culture conditions (Supplementary Material Fig. 2). However, our data do not preclude the possibility that vSMCs respond to different mechanical environments by remodeling their matrix in different ways. The response of cells to function-blocking antibodies to $\beta 1$ integrin suggests only that $\beta 1$ integrin is involved in the initial interaction of cells with both fully hydrated and dehydrated collagen films. It may be that the response of cells to the stiffer fibrils stimulates matrix remodeling with secretion of other ECM proteins that

support the observed proliferative phenotype. This possibility will be explored in future studies.

SUPPLEMENTARY MATERIAL

An online supplement to this article can be found by visiting BJ Online at <http://www.biophysj.org>.

Topographical AFM data shown in Fig. 1 was courtesy of John Woodward.

This work was funded in part by National Institute of Standards and Technology Innovative Measurement Science funding.

REFERENCES

1. Ruoslahti, E. 1996. RGD and other recognition sequences for integrins. *Annu. Rev. Cell Dev. Biol.* 12:697–715.
2. Geiger, B., A. Bershadsky, R. Pankov, and K. M. Yamada. 2001. Transmembrane crosstalk between the extracellular matrix–cytoskeleton crosstalk. *Nat. Rev. Mol. Cell Biol.* 2:793–805.
3. McCloskey, K. E., M. E. Gilroy, and R. M. Nerem. 2005. Use of embryonic stem cell-derived endothelial cells as a cell source to generate vessel structures in vitro. *Tissue Eng.* 11:497–505.
4. Paszek, M. J., N. Zahir, K. R. Johnson, J. N. Lakins, G. I. Rozenberg, A. Gefen, C. A. Reinhart-King, S. S. Margulies, M. Dembo, D. Boettiger, D. A. Hammer, and V. M. Weaver. 2005. Tensional homeostasis and the malignant phenotype. *Cancer Cell.* 8:241–254.
5. Shiu, Y. T., J. A. Weiss, J. B. Hoying, M. N. Iwamoto, I. S. Joung, and C. T. Quam. 2005. The role of mechanical stresses in angiogenesis. *Crit. Rev. Biomed. Eng.* 33:431–510.
6. Engler, A. J., M. A. Griffin, S. Sen, C. G. Bonnemann, H. L. Sweeney, and D. E. Discher. 2004. Myotubes differentiate optimally on substrates with tissue-like stiffness: pathological implications for soft or stiff microenvironments. *J. Cell Biol.* 166:877–887.
7. Lo, C. M., H. B. Wang, M. Dembo, and Y. L. Wang. 2000. Cell movement is guided by the rigidity of the substrate. *Biophys. J.* 79:144–152.
8. Chiquet, M. 1999. Regulation of extracellular matrix gene expression by mechanical stress. *Matrix Biol.* 18:417–426.
9. Roskelley, C. D., and M. J. Bissell. 2002. The dominance of the microenvironment in breast and ovarian cancer. *Semin. Cancer Biol.* 12:97–104.
10. Pelham, R. J. Jr., and Y. Wang. 1997. Cell locomotion and focal adhesions are regulated by substrate flexibility. *Proc. Natl. Acad. Sci. USA.* 94:13661–13665.
11. Dembo, M., and Y. L. Wang. 1999. Stresses at the cell-to-substrate interface during locomotion of fibroblasts. *Biophys. J.* 76:2307–2316.
12. Balaban, N. Q., U. S. Schwarz, D. Riveline, P. Goichberg, G. Tzur, I. Sabanay, D. Mahalu, S. Safran, A. Bershadsky, L. Addadi, and B. Geiger. 2001. Force and focal adhesion assembly: a close relationship studied using elastic micropatterned substrates. *Nat. Cell Biol.* 3:466–472.
13. Tan, J. L., J. Tien, D. M. Pirone, D. S. Gray, K. Bhadriraju, and C. S. Chen. 2003. Cells lying on a bed of microneedles: an approach to isolate mechanical force. *Proc. Natl. Acad. Sci. USA.* 100:1484–1489.
14. Choquet, D., D. P. Felsenfeld, and M. P. Sheetz. 1997. Extracellular matrix rigidity causes strengthening of integrin-cytoskeleton linkages. *Cell.* 88:39–48.
15. Meshel, A. S., Q. Wei, R. S. Adelstein, and M. P. Sheetz. 2005. Basic mechanism of three-dimensional collagen fibre transport by fibroblasts. *Nat. Cell Biol.* 7:157–164.
16. Elliott, J. T., A. Tona, J. T. Woodward, P. L. Jones, and A. L. Plant. 2003. Thin films of collagen affect smooth muscle cell morphology. *Langmuir.* 19:1506–1514.

17. Elliott, J. T., J. T. Woodward, K. J. Langenbach, A. Tona, P. L. Jones, and A. L. Plant. 2005. Vascular smooth muscle cell response on thin films of collagen. *Matrix Biol.* 24:489–502.
18. Langenbach, K. J., J. T. Elliott, A. Tona, D. McDaniel, and A. L. Plant. 2006. Thin films of Type 1 collagen for cell by cell analysis of morphology and tenascin-C promoter activity. *BMC Biotechnol.* 6:14.
19. Ichii, T., H. Koyama, S. Tanaka, S. Kim, A. Shioi, Y. Okuno, E. W. Raines, H. Iwao, S. Otani, and Y. Nishizawa. 2001. Fibrillar collagen specifically regulates human vascular smooth muscle cell genes involved in cellular responses and the pericellular matrix environment. *Circ. Res.* 88:460–467.
20. Henriot, P., Z. D. Zhong, P. C. Brooks, K. I. Weinberg, and Y. A. DeClerck. 2000. Contact with fibrillar collagen inhibits melanoma cell proliferation by up-regulating p27KIP1. *Proc. Natl. Acad. Sci. USA.* 97:10026–10031.
21. Mercier, I., J. P. Lechaire, A. Desmouliere, F. Gaill, and M. Aumailley. 1996. Interactions of human skin fibroblasts with monomeric or fibrillar collagens induce different organization of the cytoskeleton. *Exp. Cell Res.* 225:245–256.
22. Yoshizato, K., T. Taira, and N. Yamamoto. 1985. Growth inhibition of human fibroblasts by reconstituted collagen fibrils. *Biomed. Res. Tokyo.* 6:61–71.
23. Schor, S. L. 1980. Cell proliferation and migration on collagen substrata in vitro. *J. Cell Sci.* 41:159–175.
24. Koyama, H., E. W. Raines, K. E. Bornfeldt, J. M. Roberts, and R. Ross. 1996. Fibrillar collagen inhibits arterial smooth muscle proliferation through regulation of Cdk2 inhibitors. *Cell.* 87:1069–1078.
25. Elliott, J. T., A. Tona, and A. L. Plant. 2003. Comparison of reagents for shape analysis of fixed cells by automated fluorescence microscopy. *Cytometry A.* 52:90–100.
26. Torii, A., M. Sasaki, K. Hane, and Y. Okuno. 1995. A method for determining the spring constant of cantilevers for atomic force microscopy. *Meas. Sci. Technol.* 7:179–184.
27. Burnham, N. A., X. Chen, C. S. Hodges, G. A. Matei, E. J. Thoreson, C. J. Roberts, M. C. Davies, and S. J. B. Tendler. 2003. Comparison of calibration methods for atomic-force microscopy cantilevers. *Nanotechnology.* 14:1–6.
28. Proksch, R., T. E. Schaffer, J. P. Cleveland, R. C. Callahan, and M. B. Viani. 2004. Finite optical spot size and position corrections in thermal spring constant calibration. *Nanotechnology.* 15:1344–1350.
29. Pratt, J. R., J. A. Kramar, D. B. Newell, and D. T. Smith. 2005. Review of SI traceable force metrology for instrumented indentation and atomic force microscopy. *Meas. Sci. Technol.* 16:2129–2137.
30. Denis, F. A., P. Hanarp, D. S. Sutherland, J. Gold, C. Mustin, P. G. Rouxhet, and Y. F. Dufrene. 2002. Protein adsorption on model surfaces with controlled nanotopography and chemistry. *Langmuir.* 18: 819–828.
31. Davis, G. E. 1992. Affinity of integrins for damaged extracellular matrix: alpha v beta 3 binds to denatured collagen type I through RGD sites. *Biochem. Biophys. Res. Commun.* 182:1025–1031.
32. Jones, P. L., J. Crack, and M. Rabinovitch. 1997. Regulation of tenascin-C, a vascular smooth muscle cell survival factor that interacts with the alpha v beta 3 integrin to promote epidermal growth factor receptor phosphorylation and growth. *J. Cell Biol.* 139:279–293.
33. Reference deleted in proof.
34. Rosenblatt, J., B. Devereux, and D. G. Wallace. 1994. Injectable collagen as a pH-sensitive hydrogel. *Biomaterials.* 15:985–995.
35. Peppas, N. A. 1991. Physiologically responsive hydrogels. *J. Bioact. Compat. Polym.* 6:241–246.
36. Nottelmann, H., and W. M. Kulicke. 1991. Preparation, characterization, and rheological behavior of water-swallowable polymer networks. *ACS Symp. Ser.* 462:62–87.
37. Leikin, S., V. A. Parsegian, W. Yang, and G. E. Walrafen. 1997. Raman spectral evidence for hydration forces between collagen triple helices. *Proc. Natl. Acad. Sci. USA.* 94:11312–11317.
38. Kopp, J., M. Bonnet, and J. P. Renou. 1989. Effect of collagen crosslinking on collagen-water interactions (a DSC investigation). *Matrix.* 9:443–450.
39. Miles, C. A., T. J. Sims, N. P. Camacho, and A. J. Bailey. 2002. The role of the alpha2 chain in the stabilization of the collagen type I heterotrimer: a study of the type I homotrimer in oim mouse tissues. *J. Mol. Biol.* 321:797–805.
40. Mogilner, I. G., G. Ruderman, and J. R. Grigera. 2002. Collagen stability, hydration and native state. *J. Mol. Graph. Model.* 21: 209–213.
41. Berisio, R., L. Vitagliano, L. Mazzarella, and A. Zagari. 2000. Crystal structure of a collagen-like polypeptide with repeating sequence Pro-Hyp-Gly at 1.4 Å resolution: implications for collagen hydration. *Biopolymers.* 56:8–13.
42. Melacini, G., A. M. Bonvin, M. Goodman, R. Boelens, and R. Kaptein. 2000. Hydration dynamics of the collagen triple helix by NMR. *J. Mol. Biol.* 300:1041–1049.
43. George, A., and A. Veis. 1991. FTIRS in H₂O demonstrates that collagen monomers undergo a conformational transition prior to thermal self-assembly in vitro. *Biochemistry.* 30:2372–2377.